



ORIGINAL RESEARCH

m⁶A Regulates Neurogenesis and Neuronal Development by Modulating Histone Methyltransferase Ezh2



Junchen Chen^{1,2,#,a}, Yi-Chang Zhang^{3,4,5,#,b}, Chunmin Huang^{3,#,c}, Hui Shen^{1,2,d},
Baofa Sun^{3,4,5,6,e}, Xuejun Cheng^{1,2,f}, Yu-Jie Zhang^{2,g}, Yun-Gui Yang^{3,4,5,6,h},
Qiang Shu^{1,*,i}, Ying Yang^{3,4,5,6,*,j}, Xuekun Li^{1,2,*,k}

¹ The Children's Hospital, School of Medicine, Zhejiang University, Hangzhou 310052, China

² The Institute of Translational Medicine, School of Medicine, Zhejiang University, Hangzhou 310029, China

³ CAS Key Laboratory of Genomic and Precision Medicine, Collaborative Innovation Center of Genetics and Development, College of Future Technology, Beijing Institute of Genomics, Chinese Academy of Sciences, Beijing 100101, China

⁴ University of Chinese Academy of Sciences, Beijing 100049, China

⁵ Sino-Danish College, University of Chinese Academy of Sciences, Beijing 101408, China

⁶ Institute of Stem Cell and Regeneration, Chinese Academy of Sciences, Beijing 100101, China

Received 23 July 2018; revised 12 November 2018; accepted 21 December 2018

Available online 30 May 2019

Handled by Chengqi Yi

KEYWORDS

N⁶-methyladenosine (m⁶A);
Mettl3;
Neurogenesis;

Abstract N⁶-methyladenosine (m⁶A), catalyzed by the methyltransferase complex consisting of **Mettl3** and **Mettl14**, is the most abundant RNA modification in mRNAs and participates in diverse biological processes. However, the roles and precise mechanisms of m⁶A modification in regulating **neuronal development** and adult **neurogenesis** remain unclear. Here, we examined the function of

* Corresponding authors.

E-mail: xuekun_li@zju.edu.cn (Li X), yingyang@big.ac.cn (Yang Y), shuqiang@zju.edu.cn (Shu Q).

Equal contribution.

^a ORCID: 0000-0002-0837-570X.

^b ORCID: 0000-0001-5388-6376.

^c ORCID: 0000-0002-6124-5963.

^d ORCID: 0000-0002-8178-4614.

^e ORCID: 0000-0002-8221-1279.

^f ORCID: 0000-0002-9485-0537.

^g ORCID: 0000-0002-3202-3675.

^h ORCID: 0000-0002-2821-8541.

ⁱ ORCID: 0000-0002-4106-6255.

^j ORCID: 0000-0002-8104-5985.

^k ORCID: 0000-0002-6985-6363.

Peer review under responsibility of Beijing Institute of Genomics, Chinese Academy of Sciences and Genetics Society of China.

<https://doi.org/10.1016/j.gpb.2018.12.007>

1672-0229 © 2019 The Authors. Production and hosting by Elsevier B.V. on behalf of Beijing Institute of Genomics, Chinese Academy of Sciences and Genetics Society of China.

This is an open access article under the CC BY license (<http://creativecommons.org/licenses/by/4.0/>).

Neuronal development;
Ezh2

Mettl3, the key component of the complex, in neuronal development and adult neurogenesis of mice. We found that the depletion of *Mettl3* significantly reduced m⁶A levels in adult neural stem cells (aNSCs) and inhibited the proliferation of aNSCs. *Mettl3* depletion not only inhibited neuronal development and skewed the differentiation of aNSCs more toward glial lineage, but also affected the morphological maturation of newborn neurons in the adult brain. m⁶A immunoprecipitation combined with deep sequencing (MeRIP-seq) revealed that m⁶A was predominantly enriched in transcripts related to neurogenesis and neuronal development. Mechanistically, m⁶A was present on the transcripts of histone methyltransferase *Ezh2*, and its reduction upon *Mettl3* knockdown decreased both *Ezh2* protein expression and consequent H3K27me3 levels. The defects of neurogenesis and neuronal development induced by *Mettl3* depletion could be rescued by *Ezh2* overexpression. Collectively, our results uncover a crosstalk between RNA and histone modifications and indicate that *Mettl3*-mediated m⁶A modification plays an important role in regulating neurogenesis and neuronal development through modulating *Ezh2*.

Introduction

In the adult mammalian brain, adult neural stem cells (aNSCs) exist in specific regions, namely, the subventricular zone in lateral ventricles and the subgranular zone in the dentate gyrus of the hippocampus [1,2]. aNSCs can self-renew, and exhibit multipotent capabilities of generating neurons, astrocytes, and oligodendrocytes. The newborn neurons can integrate into existing neural circuits such as those involved in physiological functions including learning and memory [2–4]. Recent studies have shown that epigenetic modifications, such as DNA modifications, histone modifications, and non-coding RNAs, play essential roles in regulating neurogenesis and neuronal development [5–11].

N⁶-methyladenosine (m⁶A) modification is the most abundant RNA modification in the mRNAs of eukaryotic cells. It is involved in a variety of biological processes including the translation efficiency, degradation, subcellular localization, alternative splicing, and secondary structure of RNA [12–21]. m⁶A is deposited by methyltransferase-like 3 (*Mettl3*) and several other components of the methyltransferase complex. It is recognized by its YT521-B homology (YTH) domain-containing proteins and hnRNPA2B1, and is erased by the fat mass and obesity-associated protein (*Fto*) and the α -ketoglutarate-dependent dioxygenase *Alkbh5* homolog 5 (*Alkbh5*). Many studies have revealed that the modulation of m⁶A level is involved in diverse processes including the regulation of fate determination, the proliferation and differentiation of stem cells, homeostasis, DNA damage response, adipogenesis, spermatogenesis, and circadian clock processes [14,18,22–25].

Recently, it has been found that m⁶A is prevalent in mRNAs of the mammalian nervous system, and displays dynamic features during embryonic and postnatal neuronal development [16]. m⁶A eraser *Fto*-deficient mice display impaired neuronal activity and altered behaviors related to dopamine signaling [26–28]. In addition, the specific knockdown of *Fto* in the mouse medial prefrontal cortex (mPFC) can promote cued fear memory [29]. Our previous study has also found that the constitutive deletion of *Fto* inhibits adult neurogenesis *in vivo*, and impairs spatial learning and memory in mice [30]. Recently, it has been revealed that m⁶A modification regulates axon development [31,32], and the deletion of *Mettl14* or *Mettl3* dysregulates embryonic cortical neurogenesis [17,33], postnatal cerebellar development [34], and stress responses in mice [35]. All of these studies suggest important

functions of m⁶A modification in the neuronal system. However, the mechanistic role of m⁶A in regulating the proliferation and differentiation of aNSCs remains largely unknown.

In the present study, we found that both *Mettl3* and m⁶A exhibit dynamic and conservative patterns during the differentiation of aNSCs *in vitro*. *Mettl3* depletion significantly reduced m⁶A level and altered the proliferation and cell cycle progression of aNSCs. *Mettl3* depletion also skewed the lineage commitment more toward glia, and inhibited morphological maturation of newborn neurons both *in vitro* and *in vivo*. m⁶A immunoprecipitation combined with deep sequencing (MeRIP-seq) has revealed that m⁶A tags are predominantly enriched in transcripts related to neurogenesis and neuronal development. *Mettl3* depletion specifically dysregulates the expression of genes related to the cell cycle and neuronal development. Finally, we show that *Mettl3* depletion reduces the levels of histone methyltransferase *Ezh2* and H3K27me3. The overexpression of *Ezh2* could rescue the defective neurogenesis and neuronal development caused by *Mettl3* depletion. Our results thus uncover a crosstalk between RNA methylation and histone modifications and demonstrate the regulatory role of m⁶A modification in aNSC proliferation and differentiation.

Results

Mettl3 and m⁶A display dynamic expressions during aNSC differentiation

To investigate the role of *Mettl3* in NSC differentiation and neural development, we first isolated aNSCs from the forebrains of adult (2-month-old) wild-type (WT) mice, as described in our previous publications [36,37]. The cultured aNSCs were positive for the neural stem cell markers *Sox2* and *Nestin* (Figure S1A), and could incorporate thymidine analog 5-bromo-2-deoxyuridine (BrdU) during the proliferation (Figure S1B and C). aNSCs generated β -III tubulin positive (Tuj1⁺) neurons and glial fibrillary acidic protein positive (GFAP⁺) astrocytes upon differentiation (Figure S1D). mRNA levels of multiple pluripotency markers and lineage-specific markers underwent significant alterations during the processes from proliferation to differentiation (Figure S1E). These results indicate the homogeneity, self-renewal capability, and multipotency of the cultured aNSCs.

We then examined the expression of *Mettl3* in aNSCs. We first performed immunofluorescence staining using *Mettl3* and

Mettl14 specific antibodies, and found that Mettl3 and Mettl14 resided in the nuclei of Nestin⁺/Sox2⁺ aNSCs (Figure 1A and B; Figure S2A and B). Mettl3 and Mettl14 could also be detected in Tuj1⁺ neuronal cells and GFAP⁺ glial cells differentiated from aNSCs (Figure 1C and D; Figure S2C and D). Real-time PCR (RT-PCR) and Western blot results showed a significant increase in the expression of Mettl3 and Mettl14 during aNSC differentiation (Figure 1E–H; Figure S2E). During aNSC differentiation, the expression levels of *Wtap*, which encodes one component of the m⁶A writer complex, and *Fto*, which encodes an m⁶A eraser, were all increased, whereas the expression of *Alkbh5*, which encodes another m⁶A eraser, did not show any significant change (Figure S2F).

Given the dynamic expression of *Mettl3*, we then performed an RNA dot-blot assay to detect m⁶A level. Consistent with the expression pattern of *Mettl3*, we found that the global m⁶A level significantly increased from the proliferation to differentiation stages of aNSCs (Figure 1I and J). Immunostaining also showed that m⁶A existed in the mature neurons (NeuN⁺) of the hippocampus of the mouse brain (Figure S2G), which could be significantly depleted by RNase treatment. These results suggest the specificity of the m⁶A antibody (Figure S2H).

***Mettl3* regulates the proliferation and differentiation of aNSCs**

We next aimed to study the regulatory roles of *Mettl3* in the proliferation and differentiation of aNSCs. We adopted a lentivirus to deliver a short hairpin RNA (shRNA) to knock down *Mettl3* (*Mettl3* KD) in mouse aNSCs (Figure 2A and B). The dot-blot of m⁶A showed that *Mettl3* depletion significantly decreased global m⁶A levels compared to those of the control group (Figure 2C and D). To assess the effect of *Mettl3* deficiency on the proliferation of aNSCs, we first applied a BrdU incorporation assay and found that the number of BrdU⁺ cells was significantly decreased in *Mettl3* KD aNSCs (Figure 2E–G), suggesting the inhibited proliferation of aNSCs. It was noticed that the percentage of Sox2⁺/Nestin⁺ cells and the numbers of cell cycle marker Ki67⁺ cells had not changed upon *Mettl3* KD (Figure S3A–F). Taken together, these data suggest that *Mettl3* deficiency inhibits the proliferation of aNSCs but does not affect their homogeneity.

To further examine the effects of *Mettl3* on the proliferation of aNSCs, we analyzed the expression of multiple cyclins. We found that the mRNA levels of *Cyclin D1* and *D2*, which express throughout the whole cell cycle, did not show any obvious differences between control and *Mettl3* deficient cells (Figure 2H). However, the mRNA levels of *Cyclin A1*, *A2*, *B1*, *B2*, which are specifically expressed in the G2/M phase, were significantly decreased in *Mettl3* deficient aNSCs compared to those of control cells (Figure 2H). Furthermore, we used flow cytometry to analyze the distribution of cells in each phase of the cell cycle. We found that the lack of *Mettl3* increased the number of cells in S phase, but decreased the number of cells in G2/M phase (Figure 2I–K). The quantification of phosphor-histone H3 (p-H3) immunofluorescence staining showed a consistently decreased number of p-H3⁺ cells (Figure S3G). These results indicate that *Mettl3* deficiency dysregulates cell cycle progression.

We next studied the roles of *Mettl3* in regulating the differentiation of aNSCs. Immunofluorescence staining showed that *Mettl3* depletion decreased the number of Tuj1⁺ neurons (Figure 3A and B), but the overexpression of *Mettl3* significantly increased the number of Tuj1⁺ neurons upon the differentiation of aNSCs for 2 days (Figure 3C–E). The results of qRT-PCR and Western blots consistently showed that the depletion of *Mettl3* decreased the level of Tuj1 and increased the level of GFAP (Figure 3F; Figure S4A), and that the overexpression of *Mettl3* led to increased Tuj1 levels and decreased GFAP levels (Figure 3G; Figure S4B).

To further validate the effects of *Mettl3* in regulating aNSC differentiation, we applied a dual luciferase reporter assay to analyze the promoter activity of the neuronal cell marker, *NeuroD1*, and glial cell marker, *Gfap*, in aNSCs. It was found that the overexpression of *Mettl3* could increase the promoter activity of *NeuroD1* and decrease the promoter activity of *Gfap* (Figures S4C and D). To further determine the function of *Mettl3* in neuronal development, we also performed *in utero* electroporation. It was found that the percentage of new born non-neuronal cells (Tuj1⁻GFP⁺/GFP⁺) had significantly increased, meaning the significant decrease in Tuj1⁺GFP⁺ cells, in the cortical plate of *Mettl3* KD mice (Figure S4E and F). These results demonstrate that *Mettl3* regulates lineage commitment during aNSC differentiation, with a preference toward a neuronal fate.

Mettl3* regulates neuronal development both *in vitro* and *in vivo

To assess the effect of *Mettl3* on neuronal development, we further analyzed the morphology of newly born neurons generated upon the differentiation of aNSCs. We observed that both the number of dendritic branches and the total length of dendrites were significantly decreased in new born neurons after *Mettl3* KD (Figure 3H–K; Figure S4G), while they were significantly increased upon *Mettl3* overexpression (Figure 3H–K; Figure S4H). We also performed *Mettl3* KD on cultured hippocampal neurons, and found that *Mettl3* deficient neurons showed a decreased number of intersections and dendrites, a reduced total length of dendrites, and an increased mean length of dendrites (Figure 3L–O; Figure S4I). Knocking down of *Mettl3* by *in utero* electroporation consistently resulted in the number of dendrites per neuron also being significantly decreased and the mean length of dendrites being increased (Figure 3P–R). These results suggest that *Mettl3* promotes neuronal development both *in vitro* and *in vivo*.

m⁶A modified transcripts are involved in neurogenesis and neuronal development

To systematically illuminate the function of m⁶A in neurogenesis and neuronal development, we performed m⁶A immunoprecipitation combined with deep sequencing (MeRIP-seq) to detect the m⁶A peaks and explore their distribution in the transcriptome of aNSCs under proliferation and differentiation conditions (Figure S5A). We observed in both proliferating and differentiated aNSC samples that the m⁶A peaks were predominantly located in the coding sequence (CDS) and that the 3' untranslated regions (3'UTR) were especially enriched near stop codon regions (Figure 4A and B). The m⁶A distribution

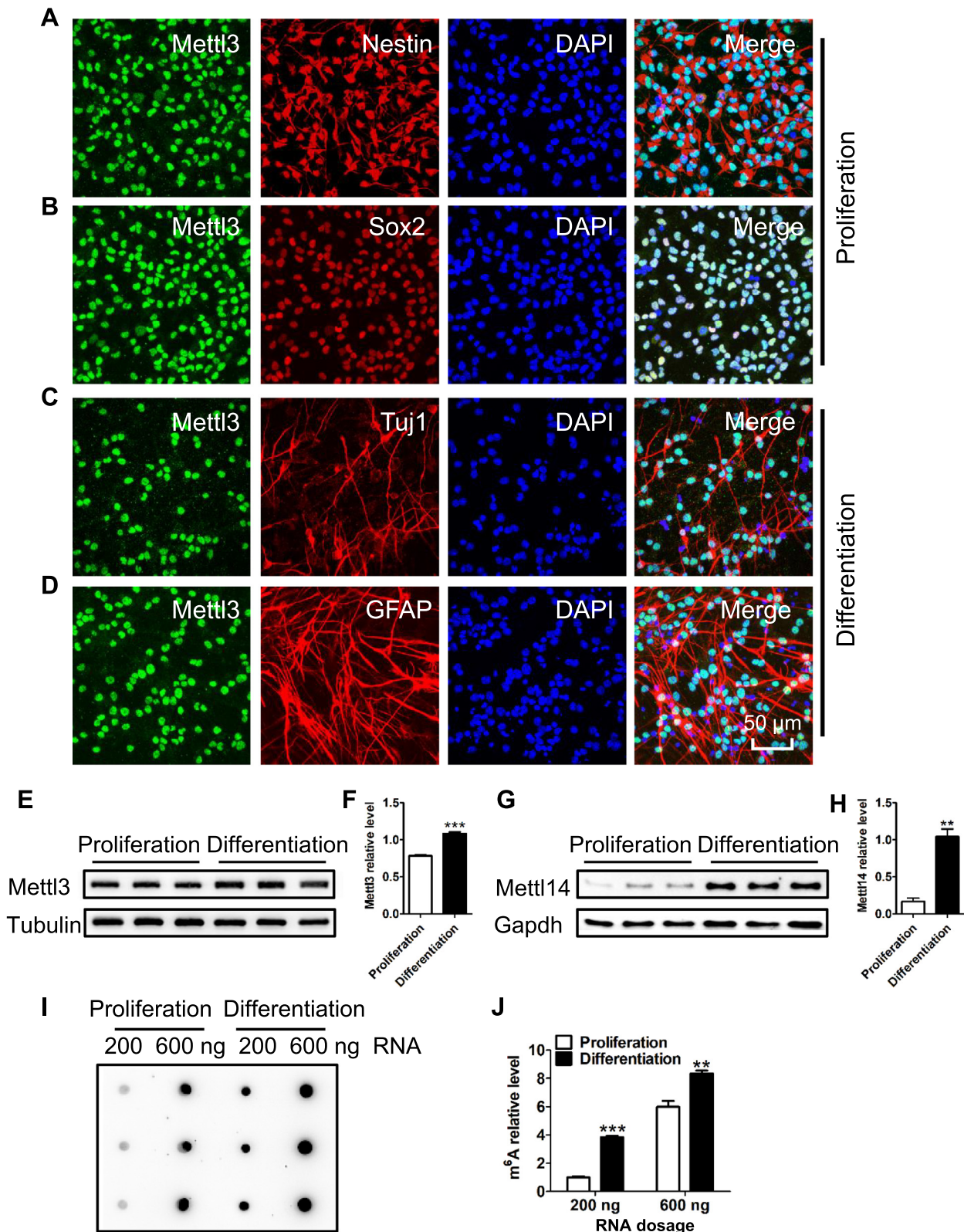


Figure 1 The dynamic expression of *Mettl3* and *m*⁶A during the differentiation of aNSCs

Representative immunostaining showing the expression of *Mettl3* in Nestin⁺ (A) and Sox2⁺ (B) aNSCs. Immunofluorescence staining showing the expression of *Mettl3* in Tuj1⁺ neuronal cells (C) and GFAP⁺ astrocytes (D). Western blot (E) and quantification (F) showing the increased expression of *Mettl3* upon the differentiation of aNSCs ($n = 3$). Western blot (G) and quantification (H) showing the increased expression of *Mettl14* upon the differentiation of aNSCs ($n = 3$). Tubulin and Gapdh were used as loading controls. Dot-blot assay (I) and quantification (J) revealing the increase in *m*⁶A levels upon the differentiation of aNSCs ($n = 3$). Data are presented as mean \pm SEM. Unpaired *t*-test, **, $P < 0.01$; ***, $P < 0.001$. Scale bar, 50 μ m. aNSC, adult neural stem cell; Tuj1, β -III tubulin; GFAP, glial fibrillary acidic protein.

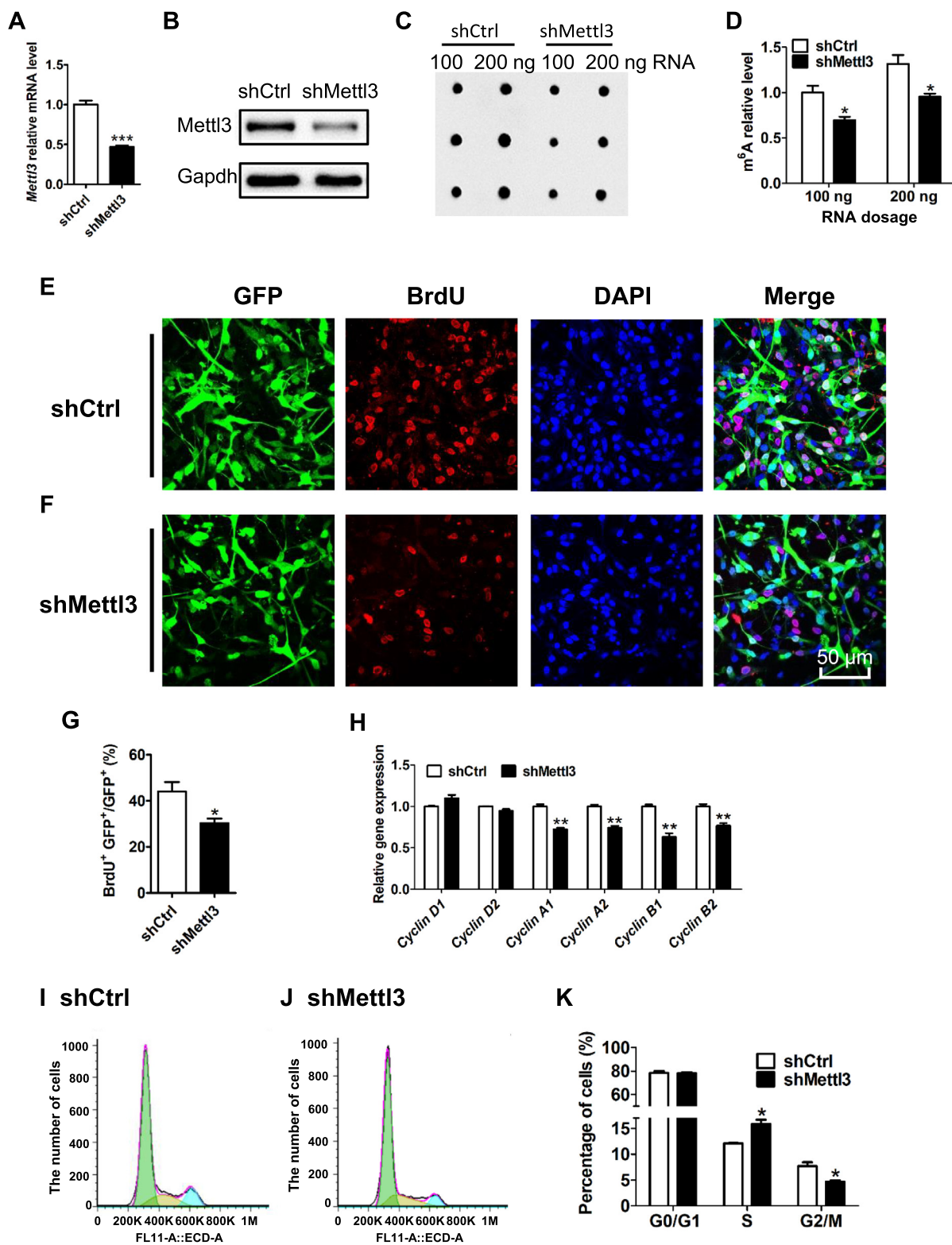


Figure 2 *Mettl3* regulates the proliferation of aNSCs

RT-PCR results showing the mRNA levels of *Mettl3* in control and *Mettl3* KD aNSCs (A). *Actin* was used as an internal control ($n = 3$). Western blot assays showing decreased *Mettl3* in *Mettl3* KD aNSCs compared to control samples (B). *Gapdh* was used as internal control. Dot-blot assay (C) and quantification (D) revealing the depletion of m^6A in *Mettl3* KD aNSCs compared to the control samples ($n = 3$). Representative images of BrdU immunostaining in both control (E) and *Mettl3* deficient (F) aNSCs. The quantification analysis of BrdU immunostaining in control and *Mettl3* KD aNSCs ($n = 3$) (G). The expression levels of multiple cyclin genes in control and *Mettl3* KD aNSCs were detected by qRT-PCR (H) ($n = 3$). *Actin* was used as an internal control. Flow cytometry analysis of the cell cycle status of control (I) and *Mettl3* KD aNSCs (J), and the percentage in each phase (K) ($n = 3$). Data are presented as mean \pm SEM, unpaired *t*-test, *, $P < 0.05$; **, $P < 0.01$; ***, $P < 0.001$. Scale bar, 50 μ m. BrdU, 5-bromo-2-deoxyuridine; KD, knockdown.

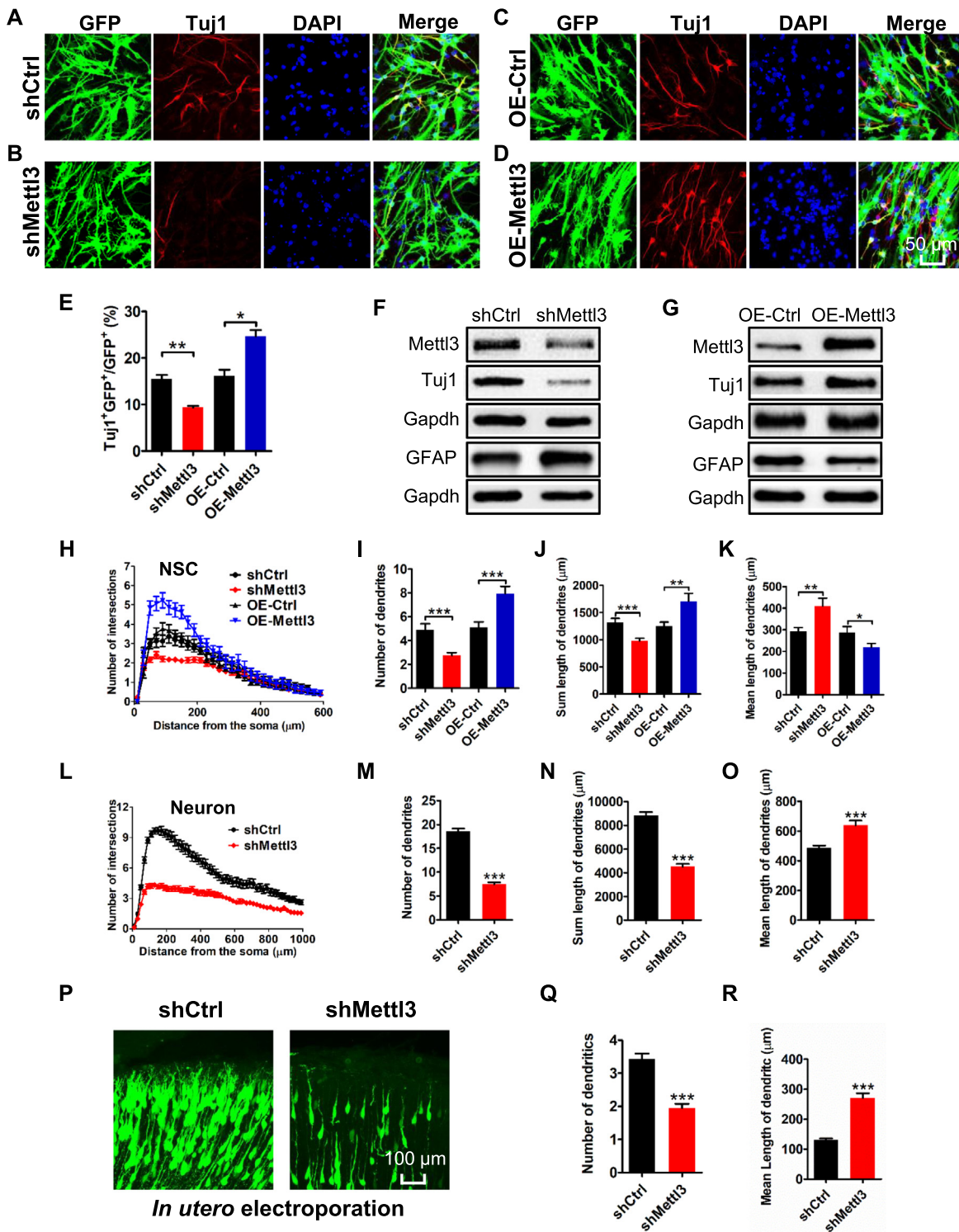


Figure 3 *Mettl3* regulates the differentiation and neuronal development of aNSCs

Representative immunofluorescence images of the differentiated aNSCs with neuronal cell marker TuJ1 of control (A, C), *Mettl3* KD (B), and *Mettl3* OE (D) groups. Scale bar, 50 μm. Quantification of TuJ1⁺ cells in differentiated aNSCs with *Mettl3* KD and *Mettl3* overexpression ($n = 3$) (E). Western blot assays showing the protein levels of the neuronal cell marker, TuJ1, and astrocyte marker, GFAP, in aNSCs (differentiation condition) with *Mettl3* KD (F) and *Mettl3* overexpression (G). Sholl analysis of newborn neurons generated upon the differentiation of aNSCs (H–K) ($n = 40$). Sholl analysis of cultured hippocampal neurons (L–O) (control group: $n = 75$; KD group: $n = 66$). Representative images of *in utero* electroporation (P). The quantifications of the number (Q) and length (R) of dendrites. Data are presented as mean ± SEM, unpaired *t*-test, *, $P < 0.05$; **, $P < 0.01$; ***, $P < 0.001$. Scale bar, 50 μm. OE, overexpression.

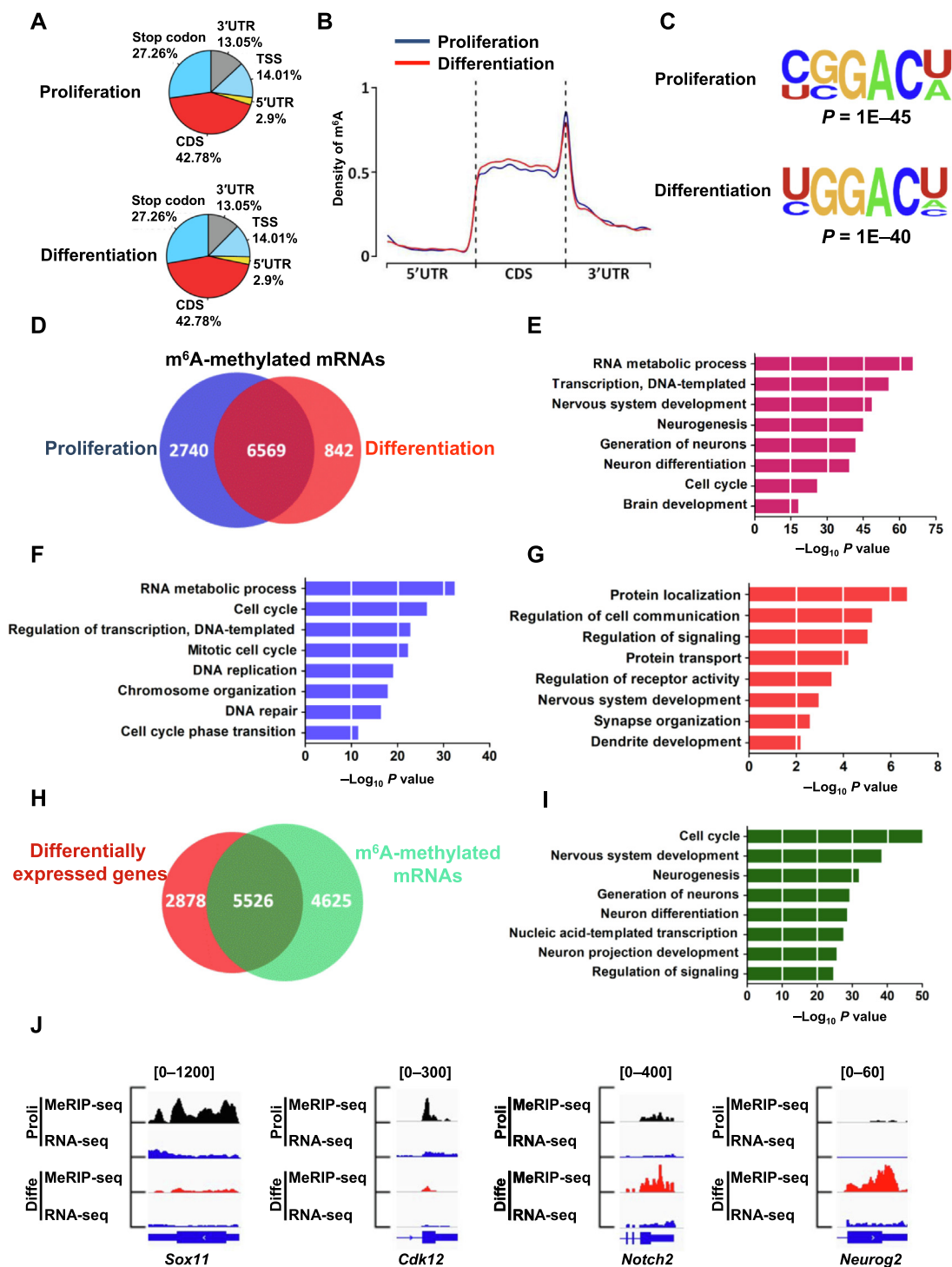


Figure 4 Dynamic m⁶A modification from proliferation to differentiation of aNSCs

Transcriptome-wide distribution of m⁶A peaks in aNSCs under the conditions of proliferation and differentiation (A, B) ($n = 2$). The most common sequence motif among m⁶A peaks during proliferation and differentiation (C). Venn diagram illustrating the m⁶A modified genes in proliferating and differentiated samples (D). GO analysis of the common m⁶A modified genes shared between proliferating and differentiated samples (E). GO analysis of the m⁶A modified specific genes identified in proliferating samples (F) and differentiated samples (G). Venn diagram illustrating the total m⁶A-tagged genes identified in proliferating and differentiated samples, and differentially expressed genes identified in differentiated samples compared to proliferating samples (H). GO analysis of the common genes shared between m⁶A tagged genes and differentially expressed genes (I). IGV tracks showing several genes with differential m⁶A modification from the proliferation to differentiation of aNSCs (J). RNA-seq reads were used as input. TSS, transcription start site; GO, Gene Ontology; Proli, proliferation; Diffe, differentiation; IGV, Integrative Genomics Viewer.

pattern displayed a high degree of similarity between proliferation and differentiation conditions, and was enriched in the m⁶A consensus motif, which was consistent with previous reports [15,18] (Figure 4C). Bioinformatic analysis revealed that 9309 and 7411 m⁶A methylated mRNAs were detected in proliferation and differentiation conditions, respectively (Table S1), whereas 6569 m⁶A methylated mRNAs overlapped between the two conditions (Figure 4D). Gene ontology (GO) analysis showed the functional enrichment of these 6569 overlapped genes was related to the transcription, neurogenesis, neuronal differentiation and cell cycle related pathways (Figure 4E). Furthermore, 2740 unique m⁶A methylated RNAs in proliferating samples were enriched in terms related to DNA replication and the cell cycle, while 842 unique m⁶A methylated genes in differentiated samples were enriched in terms related to neurogenesis, neuronal development and differentiation (Figure 4F and G).

To determine the relationship between m⁶A modification and gene expression, we next performed RNA-seq in these two conditions to uncover any global transcriptome alterations (Figure S5B). It was found that 8404 genes displayed altered expression from proliferation to differentiation conditions of aNSCs: 4378 (52.09%) mRNAs were up-regulated while 4026 (47.91%) genes were down-regulated (Table S2). Among these 8404 genes, 5526 (65.75%) genes were modified by m⁶A, including 3065 (55.47%) up-regulated genes and 2461 (44.53%) down-regulated genes (Figure 4H; Table S3). GO analysis showed that these 5526 genes were enriched in pathways related to the cell cycle, nervous system development and neuronal differentiation (Figure 4I). Key examples include, *Sox11* and *Cdk12*, involved in proliferation, and *Notch2* and *Neurog2*, related to neuronal differentiation (Figure 4J; Figure S5C). Taken together, these data suggest that m⁶A modification plays a key role in regulating the gene expressions of aNSCs.

Mettl3 regulates m⁶A modification of neurogenesis-related genes

Given that *Mettl3* regulates neurogenesis and neuronal development, we next sought to investigate whether *Mettl3* KD affected gene expression related to those two areas. We first examined m⁶A distribution patterns in control and *Mettl3* KD aNSCs (in a proliferation condition) (Figure S5A), and observed that *Mettl3* KD had not altered the overall m⁶A distribution patterns in transcripts compared to those of the control samples (Figure 5A). Furthermore, m⁶A was enriched in the same m⁶A consensus motifs of both *Mettl3* KD and control samples, even though the global m⁶A level had been significantly decreased (Figure 2C; Figure 4C; Figure 5A).

To examine the effects of *Mettl3* depletion on gene expression, we performed RNA-seq in control and *Mettl3* KD samples (a proliferating condition) (Figure S5B). RNA-seq data analysis showed that a total of 1226 genes exhibited altered expressions in *Mettl3* KD samples compared with those of control samples (Fold change > 1.5), including 844 (68.84%) up- and 382 (31.16%) down-regulated genes (Figure 5B; Table S4). Among the up-regulated genes, 371 genes (43.96%) were methylated by m⁶A, while 176 down-regulated genes (46.07%) were methylated by m⁶A (Figure 5B and C). GO analysis showed that the m⁶A tagged up-regulated genes were enriched in areas of neuronal differentiation,

neurogenesis and nervous system development (Figure 5D and E). The representative IGV images showed that m⁶A tagged down-regulated genes were enriched in terms related to the neuronal development, such as *Vegfa* and *Syt4*, and cell cycle, cell proliferation, such as *Tet1* and *E2f7* (Figure 5F). The analysis using STRING database showed the interaction between proteins coded by m⁶A tagged transcripts (Figure 5G). Meanwhile, we also performed GO analysis of differentially expressed genes without m⁶A modification, and found that these genes showed low correlations with neuronal development and the cell cycle (Figure S5E and F). Together, these results suggest that altered m⁶A modification induced by *Mettl3* depletion impacts the expression of genes related to cell cycle progression and neuronal development.

Ezh2 rescues the deficits of neuronal development and neurogenesis induced by Mettl3 depletion

One recent study has shown that m⁶A regulates specific histone modifications [38]. Through analyzing m⁶A sequencing data, we observed that the transcripts of histone methyltransferase *Ezh2*, which plays important roles in neurogenesis and neuronal development [37,39,40], were tagged with m⁶A modification (Figure S6A). The region with the largest m⁶A peak was on exon 10 of *Ezh2* and this was validated by m⁶A RIP followed by qPCR (Figure S6B). m⁶A enrichment at *Ezh2* was significantly decreased upon *Mettl3* depletion, as confirmed by m⁶A-IP-qPCR (Figure S6C). Western blot results showed that the protein level of *Ezh2* was significantly decreased upon *Mettl3* depletion, whereas its mRNA level did not change (Figure 6A and B; Figure S6D). Consistently, the protein level of H3K27me3 was also decreased after *Mettl3* depletion while no observable changes were noted in the levels of H3K4me3 (Figure 6C). We further constructed a mutant *Ezh2* plasmid (the site within the biggest m⁶A peak on exon 10 was denoted in Figure S6A and was mutated). The overexpression of WT or mutant *Ezh2* showed similar transcription efficiencies (Figure S6E and G), and neither of them were observed to affect any protein and mRNA levels of *Mettl3* in either aNSCs or N2a cells (Figure S6F; Figure S6H and I). Consistent with the effects of *Mettl3* KD on the expression of *Ezh2*, *Mettl3* overexpression not only significantly increased the global level of m⁶A, but also upregulated the levels of *Ezh2* and H3K27me3 (Figure S6J–L). These results suggest that *Mettl3* regulates *Ezh2*, but not *vice versa*.

Next, we analyzed the effect of knocking down *Mettl3* on the expression of exogenous *Ezh2*. We found that the protein levels of both endogenous and exogenous WT *Ezh2* were significantly decreased upon *Mettl3* KD (Figure 6D and E), while mRNA levels remained unaltered (Figure S6D). However, *Mettl3* knockdown exhibited less effect on the protein level of mutated *Ezh2* (Figure 6D and E). Together, these results suggested *Mettl3* deposited m⁶A modification regulates *Ezh2* expression at the translational level.

We finally examined whether *Ezh2* could rescue the deficits of aNSCs induced by *Mettl3* depletion. The results showed that the overexpression of *Ezh2* could increase proliferation (indicated by the number of BrdU⁺ cells) (Figure 6F and G) and promote neuronal differentiation (indicated by the number of Tuj1⁺ cells) of aNSCs induced by *Mettl3* KD (Figure 6H and I). Furthermore, the dendritic number and

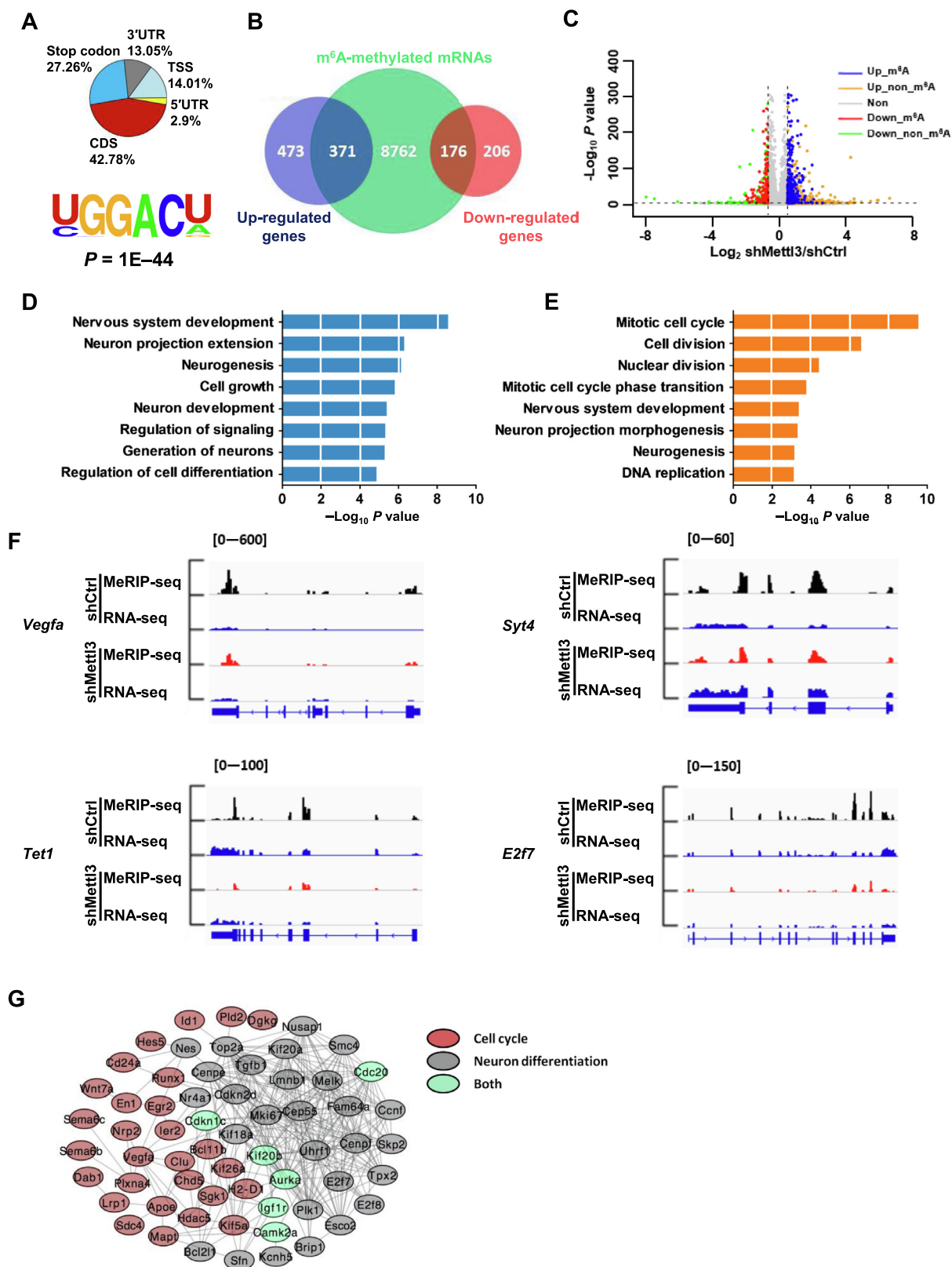


Figure 5 Mettl3-mediated m⁶A regulates gene expression in proliferating aNSCs

Transcriptome-wide distribution of m⁶A peaks in *Mettl3* KD samples ($n = 2$) (A). Venn diagram illustrating the up-regulated and down-regulated transcripts and m⁶A-modified transcripts in *Mettl3* KD samples (B). Volcano plot showing differentially expressed genes between control and *Mettl3* KD samples (C). GO analysis of m⁶A-tagged up-regulated (D) and down-regulated (E) transcripts in *Mettl3* KD samples. Four examples of IGV tracks showing that the enrichment of m⁶A in several transcripts, which are related to neurogenesis and neuronal development, were significantly decreased in *Mettl3* KD samples (F). RNA-seq reads were used as input. The interaction network showing differentially expressed transcripts with m⁶A modification. Genes related to cell cycle and neuronal differentiation are marked in red and gray, respectively, whereas genes related to both processes are marked in green (G).

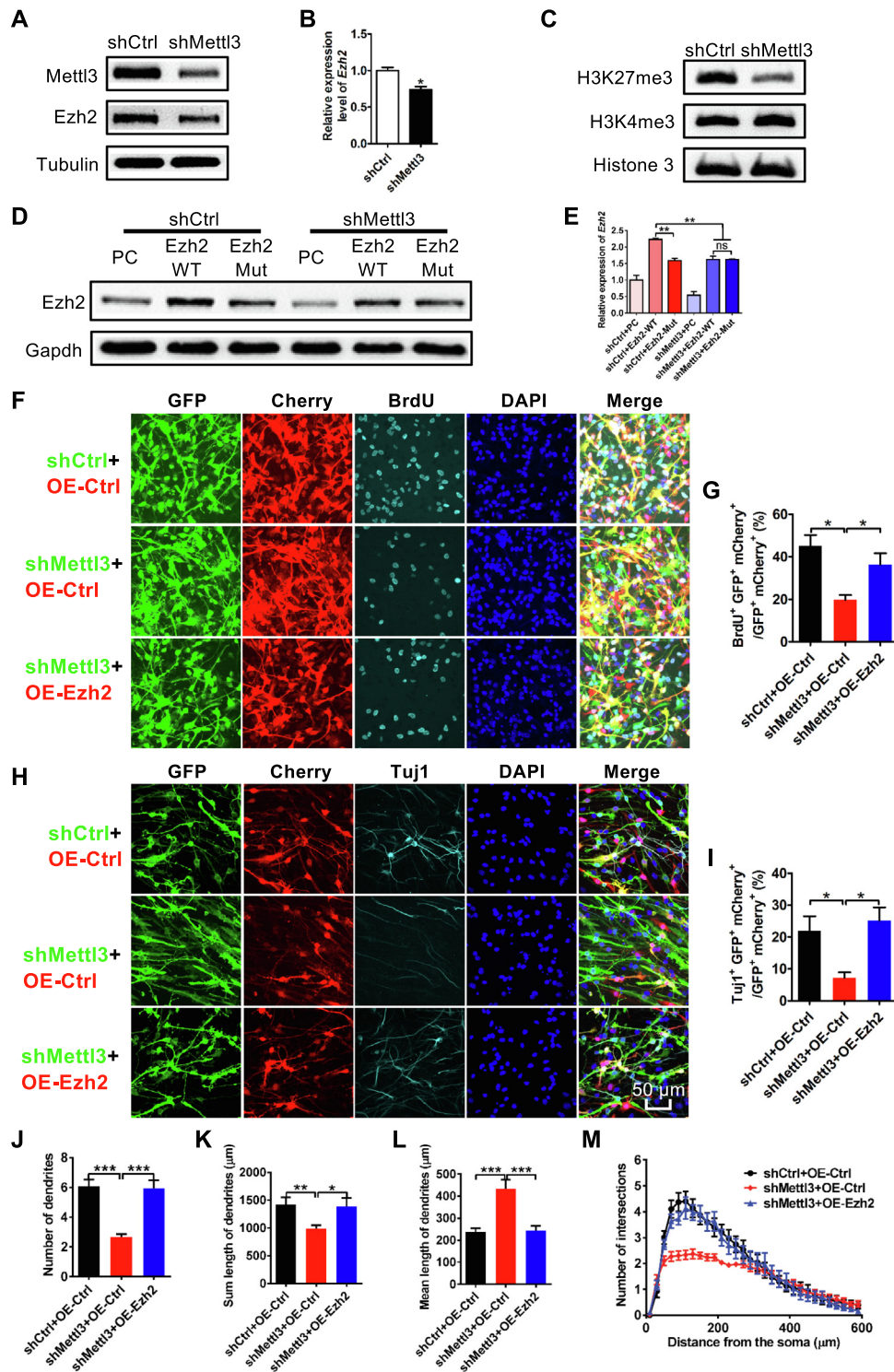


Figure 6 Ezh2 is regulated by Mettl3 and can rescue the deficits of neuronal development and neurogenesis induced by *Mettl3* knockdown. Western blot assay showing *Mettl3* KD led to a significant decrease in Ezh2 (A, B), and H3K27me3 (C) at the protein level ($n = 3$). Western blot assay (D) and quantification (E) showing that *Mettl3* KD significantly decreased expression of WT Ezh2, but had less effect on the expression of mutant Ezh2 ($n = 3$). Representative images (F) and quantification (G) showing that the overexpression of *Ezh2* rescued the reduced proliferation induced by *Mettl3* KD ($n = 3$). Representative images (H) and quantification (I) showing that the overexpression of *Ezh2* rescued the inhibited neuronal differentiation induced by *Mettl3* KD ($n = 3$). *Ezh2* rescued the impaired morphological maturation of newborn neurons induced by *Mettl3* KD ($n = 30$) (J–M). Data are presented as mean \pm SEM, unpaired *t*-test, *, $P < 0.05$; **, $P < 0.01$; ***, $P < 0.001$. Scale bar, 50 μ m.

length, and the number of intersections of new born neurons, were also increased upon *Ezh2* overexpression (Figure 6J–M). Taken together, these results indicate that overexpression of *Ezh2* could rescue the deficits of neurogenesis and neuronal development induced by *Mettl3* depletion.

Discussion

Adult neurogenesis is a multi-step event involving the maintenance of the stem cell pool, lineage commitment, maturation, and the establishment of neural circuits. All of these processes are precisely and intensively regulated by genetic and epigenetic mechanisms. Here, we have demonstrated the important roles of *Mettl3*-mediated m⁶A methylation in regulating the neurogenesis and neuronal development through modulating the expression of histone methyltransferase *Ezh2* (Figure S6M).

m⁶A has been shown to modulate the self-renewal, differentiation, and lineage determination of multiple stem cell types by regulating gene expression, especially the expression of key transcription regulators [18,23,25,41,42]. The distribution pattern of m⁶A is highly conservative with an abundance in 3'UTRs and near the stop codons observed across different cell types [16,18,19]. Our results have shown that, in the transcriptomes of aNSCs, m⁶A exhibits similar distribution features, and is enriched at similar motifs. These highly conservative features of m⁶A modification indicate its important function in different cell types.

Dynamic m⁶A modification has not only been found during neuronal development, but also can be induced by neuronal activity and learning, pointing to the function of m⁶A in the neuronal system [16,26,27,29,43]. Our previous study showed that the deletion of *Fto* inhibits adult neurogenesis as well as learning and memory through its regulation of *BDNF* [30]. The deletion of either *Mettl3*, *Mettl14*, or *Ythdf2* could disturb embryonic cortical neurogenesis in mice [17,33]. Ectopic expression of *Mettl3* induced neuronal defects in the cerebellum [34]. Our present results indicate that *Mettl3* depletion not only inhibits the proliferation and cell cycle progression of aNSCs, also skews their lineage commitment more toward glia during the differentiation *in vitro*. Moreover, our study also showed that m⁶A modification regulates the morphological development of neurons. We found that, besides the RNAs tagged by m⁶A that are highly overlapping between proliferation and differentiation conditions, m⁶A also specially tags unique mRNAs under either proliferation or differentiation conditions. It is plausible to speculate that the dynamic and specific distribution patterns of m⁶A tagging on transcripts are highly correlated to its function in aNSCs. In this way, these results further highlight the function of m⁶A modification in neuronal development and adult neurogenesis.

The roles exactly played by m⁶A modification are under intensive study. Previous studies have reported that m⁶A regulates gene expression through modulating splicing and the efficiency of translation [19,44–46]. Although *Mettl14* itself does not have catalytic activity, the deletion of *Mettl14* could significantly reduce global m⁶A levels, disturb embryonic cortical neurogenesis, impair striatal-mediated behavior and function through affecting global transcriptomes [17,47]. All these studies indicate the roles of RNA methyltransferase-mediated m⁶A in regulating gene expression during development and during

the operation of various physiological functions such as that of neuronal function. One recent study has indicated that m⁶A modification affects histone modification. *Mettl14* haploinsufficiency led to genome-wide changes in histone modification including increased H3K27me3, H3K27ac, and H3K4me3 [38]. However, we observed that the level of the methyltransferase *Ezh2* was significantly decreased in *Mettl3* deficient cells, while its overexpression could rescue *Mettl3* deficiency induced phenotypes. Whether this discrepancy was due to the specific cell types under study requires further examination.

In summary, our study has revealed the critical roles of *Mettl3*-mediated m⁶A modification in regulating cell cycle progression, lineage commitment and neuronal development of aNSCs through modulating histone methyltransferase *Ezh2*. These findings highlight the function of epitranscriptomic mechanisms in neuronal development and adult neurogenesis.

Materials and methods

Animals

Mice were housed in standard conditions in the Laboratory Animal Center of Zhejiang University on a 12 h light/dark schedule with free access to food and water. The pregnant mice were purchased from Shanghai SLAC Laboratory Animal Company, China. All animal experiments were conducted according to protocols approved by the Zhejiang University Animal Care and Use Committee.

Isolation and culture of aNSCs

The isolation of NSCs from the forebrain of adult mice was performed as described previously [36,37]. aNSCs were cultured in DMEM/F-12 medium containing 20 ng/ml FGF-2 (Catalog No. 100-18B-B; PeproTech, Rocky Hill, NJ), 20 ng/ml epidermal growth factor (Catalog No. 100-15; PeproTech), 2% B27 supplement (Catalog No. 12587-010; Thermo Fisher Scientific, Grand Island, NY), 1% antibiotic–antimycotic (Catalog No. 15140-122; Thermo Fisher Scientific), and 2 mM L-glutamine (Catalog No. 25030-149; Thermo Fisher Scientific) in a 5% CO₂ incubator at 37 °C.

In vitro proliferation and differentiation assay

For the *in vitro* proliferation assay, aNSCs were cultured on coverslips with medium supplied with 5 μM BrdU for 8 h. For the *in vitro* differentiation assay, aNSCs were cultured on coverslips with proliferation medium, and then transferred into differentiation medium containing 1 μM retinoic acid (Catalog No. R-2625; Sigma, Saint Louis, MO) and 5 μM forskolin (Catalog No. F-6886; Sigma) for 48 h.

Immunofluorescence staining

After washing with PBS for 30 min, cell samples on coverslips or brain sections were blocked with 3% normal goat serum and 0.1% triton X-100 in PBS for 1 h at room temperature. Samples were incubated with primary antibodies over night at 4 °C. The second day, cells or sections were washed with

PBS for 30 min, and then incubated with Fluorophore-conjugated secondary antibodies for 1 h at room temperature. For BrdU immunostaining, samples were pretreated with 1 M HCl at 37 °C for 30 min before the application of block solution. The following primary antibodies were used: Mettl3 (Catalog No. 21207-1-AP; Proteintech, Rosemont, IL), Mettl14 (Catalog No. HPA038002; ATLAS, Bromma, Sweden), m⁶A (Catalog No. 202003; Synaptic Systems, Goettingen, Germany), NeuN (Catalog No. AB2237; Millipore, Burlington, MA), Nestin (Catalog No. 556309; BD Pharmingen, San Jose, CA), SOX2 (Catalog No. sc-365823X; Santa Cruz Biotechnology, Dallas, TX, USA), Tuj1 (Catalog No. G712A; Promega, Madison, WI), GFAP (Catalog No. Z0334; DAKO, Santa Clara, CA), BrdU (Catalog No. ab6326; Abcam, Cambridge, MA), and Ki67 (Catalog No. AB9260; Millipore).

Electroporation and luciferase assays

Electroporation was performed with an electroporator (Catalog No. AAB-1001; Amaxa Lonza, Germany) as described previously [37]. Briefly, the cultured aNSCs were collected and resuspended with 100 µl nucleofection solution and electroporated using the manufacturer's protocol. The electroporated cells were cultured with fresh proliferation medium and the medium was replaced with differentiation medium (5 µM forskolin and 1 µM retinoic acid) on the second day. 48–60 h later, the cells were collected for a luciferase assay with a luminometer according to the manufacturer's protocol (Promega). 0.1 µg Renilla-luciferase plasmids and 2 µg NeuroD1-/Gfap-luciferase plasmids were used for each electroporation, respectively. To knock down *Mettl3*, short hairpin RNA (shRNA) targeting *Mettl3* (5'-taagcacactgatgatcttt-3', Qiagen, Hilden, Germany) was cloned into to lentivirus-U6 vectors.

Total RNA isolation, reverse transcription, and quantitative real-time PCR

Total RNA was extracted from aNSCs using TRIzol reagent (Catalog No. 15596018; Thermo Fisher Scientific). Total RNA was isolated and the concentration was quantified using a NanoDrop spectrophotometer 2000 (Thermo Fisher Scientific). 0.5 µg total RNA was used for reverse transcription (RT) using a RT reagent kit (Catalog No. R223-01; Vazyme, Nanjing, China). Quantitative real-time PCR (qRT-PCR) was performed using SYBR Green (Catalog No. Q71502; Vazyme). All real-time PCR reactions were performed in triplicate, and the results were analyzed using the $\Delta\Delta C_t$ method.

Western blot

The collected cells were washed with PBS and resuspended with RIPA buffer (Catalog No. ab156034; Abcam, Cambridge, MA, USA) containing 1× protease inhibitor cocktail (Catalog No. 04693124001; Sigma, Saint Louis, MO, USA). The samples were centrifuged at 4 °C for 20 min at 14,000 rpm and the supernatants were collected. Samples were then denatured for 5 min at 95 °C and then subjected to SDS-polyacrylamide gel electrophoresis. The following primary antibodies were used: anti-Mettl3 (Catalog No. 21207-1-AP; Proteintech), anti-Mettl14 (Catalog No. HPA038002;

ATLAS), anti-Tuj1 (Catalog No. G712A; Promega), anti-GFAP (Catalog No. 3670; Cell Signaling, Danvers, MA), anti-tubulin (Catalog No. ab15246; Abcam), anti-Ezh2 (Catalog No. 3147; Cell Signaling), anti-H3K27me3 (Catalog No. 07-449; Millipore), anti-H3K4me3 (Catalog No. ab8580; Abcam), anti-Histone3 (Catalog No. ab1791; Abcam), and anti-Gapdh (Catalog No. AM4300; Thermo Fisher Scientific). Secondary HRP conjugated antibodies were applied for 1 h at room temperature. The signal was detected by Tanon Detection system (Tanon 5200, Shanghai, China) and the intensity of immuno-blot bands was normalized to those of Gapdh or Tubulin.

m⁶A dot-blot assay

For m⁶A dot-blot, total RNA samples were denatured at 65 °C, and then spotted onto Hybond N⁺ membranes (Catalog No. NP1096; GE Healthcare, Buckinghamshire, UK). Membranes were blocked with 5% milk for 1 h at room temperature, and then incubated with primary antibodies overnight at 4 °C. On the next day, membranes were incubated with HRP-conjugated secondary antibodies for 30 min at room temperature. The signal was detected by Tanon Detection system, and the signal density was quantified using Photoshop software.

Cell cycle analysis

To analyze the cell cycle aNSCs, propidium iodide (PI) staining was performed according to the manufacturer's instructions (Multi Sciences, Hangzhou, China). In brief, after subculture for 24 h, aNSCs were harvested and fixed with absolute ethanol. The pellet was then dislodged in PBS and stained with propidium iodide solution at room temperature for 30 min. The cells were then analyzed using CytoFLEX (Beckman Coulter, Boulevard Brea, CA) and data were analyzed using FlowJo software.

In utero electroporation (IUE)

In utero electroporation was performed as described previously [48]. Briefly, the timed pregnant C57 mice (E13.5) were anesthetized using isoflurane. The uterine horns were then exposed and bathed in warm PBS. 2 µl recombinant plasmid (final concentration 1.5 mg/ml) mixed with fast green (0.01%) was manually microinjected into the lateral ventricle with a glass micropipette (Hirschmann DE-M 16). For electroporation, five 100-microsecond pulses of 35 V with a 900-microsecond interval were delivered across the uterus using an electroporator (Catalog No. 101438; BEX, Tokyo, Japan). After electroporation, the uterine horns were placed back into the abdominal cavity to allow the embryos to continue normal development. The pregnant mice were sacrificed at scheduled time points as indicated and the embryos were harvested for further analysis.

mRNA purification, m⁶A MeRIP-seq and m⁶A MeRIP-qPCR

m⁶A MeRIP-seq was carried out as previously described with some modifications [16,25,49]. In brief, mRNAs were purified

from total RNAs using a Dynabeads® mRNA purification kit (Catalog No. 61006; Thermo Fisher Scientific), and digested with DNase I to remove any potential DNA contamination. mRNAs were fragmented to around 100 nt using an RNA fragmentation reagent (Catalog No. AM8740; Thermo Fisher Scientific) through incubation at 90 °C for 1 min, and were then precipitated with ethanol. The m⁶A polyclonal antibody (Catalog No. 202003; Synaptic Systems) was incubated with 40 µl Dynabeads™ Protein A (Catalog No. 10001D; Thermo Fisher Scientific) in 500 µl IPP buffer (150 mM NaCl, 0.1% NP-40, 10 mM Tris-HCl, pH 7.4) for 1 h at room temperature. The recovered mRNAs were denatured at 75 °C for 5 min and put on ice immediately. 5 µg of fragmented mRNAs were added to the antibody-bead mixture followed by the incubation at 4 °C for 4 h. After extensive washing by IPP buffer five times, the m⁶A-containing RNAs were eluted for twice with 300 µl 0.5 mg/ml N⁶-methyladenosine (Catalog No. P3732; Berry & Associates, Dexter, MI) at room temperature for 1 h using gentle rotation. The eluted samples were combined together and extracted with Acid Phenol (pH 4.3–4.7), followed by standard ethanol precipitation. The recovered RNA was subjected to the cDNA library construction by using KAPA Stranded mRNA-Seq Kit Illumina® platform (Catalog No. KK8401; KAPA, Boston, MA) and sequenced on the HiSeq 3000 platform.

RNA-seq and MeRIP-seq data analysis

MeRIP-seq and RNA-seq was performed. The proliferation (proli) versus differentiation (differ) cells, and control versus *mettl3* knockdown cells were conducted in two biological replicates using an Illumina HiSeq 3000 platform. Raw reads of each sample ($n = 2$ for each group) were trimmed using the Trimmomatic software for each sample to remove adaptor sequences and bases with low quality [50]. The processed reads with length larger than 35 nt were then aligned to the mouse reference genome (version mm10, UCSC) using TopHat2 [51] with default parameters. Only unique mapped reads with mapping quality no less than 20 were kept for the subsequent analysis.

For MeRIP-seq, the MACS2 software was used to identify m⁶A-enriched (version 2.0.10) [52], with the corresponding input sample serving as control. MACS2 was run with default options except for ‘-nomodel, -keepdup all’ to turn off fragment size estimation and to keep all uniquely mapping reads, respectively. To identify high confidential or overlapped m⁶A peaks, peaks were intersected in a pairwise fashion among two replicates or between two conditions using the BedTools package by setting ‘-f 0.5’ [53]. Fold changes for m⁶A peaks were obtained from MACS2 output.

For RNA-seq, the number of reads mapped to each Ensemble gene (release 68) were counted using the HTSeq python package [54], with the ‘union’ overlap resolution mode and unstranded count feature by setting ‘--mode = union’ and ‘--stranded = no’, respectively. The expression of transcripts was quantified as reads per kilobase of exon model per million mapped reads (RPKM). These RNAs, which are methylated by m⁶A in both conditions, are defined as overlapped m⁶A methylated RNAs.

Motif identification within m⁶A peaks

Motifs enriched in m⁶A peaks within all mRNAs were identified using HOMER software (v4.7) [55]. BEDTools’ shuffleBed (version 2.16.2) was used to generate random peaks within total mRNAs as background sequences [53]. The motif length was restricted to 5–6 nucleotides.

Statistical analysis of differentially expressed genes

To identify differentially expressed genes, the R-package DEGseq was used with fold-change ≥ 1.5 , $P \leq 1 \times 10^{-3}$ and the method MARS (MA-plot-based method with random sampling model) as the parameters [56].

Gene ontology analysis

Gene ontology (GO) analysis was performed using the DAVID database [57]. Enrichment maps were generated by Cytoscape (version 3.5.0) with the Enrichment Map plugin [58]. Each enriched GO function term is represented by a node and the node size is proportional to the number of genes in its corresponding function term in the enrichment maps. The thickness of each edge represents the number of common genes between two linked nodes. Similar GO functions are categorized as one cluster. The function term and the number of genes in each cluster are labeled. A gene interaction network was generated using STRING [59].

Statistical analysis

All data are expressed as mean \pm SEM. GraphPad Prism (GraphPad Software Inc.) was used for statistical analysis. Unpaired student’s *t*-test was used to determine the differences between two groups; a two-way ANOVA analysis followed by Bonferroni multiple-comparison test was used to determine differences between multiple groups. $P < 0.05$ was considered statistically significant.

Data availability

The raw sequence data reported in this paper have been deposited in the Genome Sequence Archive [60] in BIG Data Center [61], Beijing Institute of Genomics (BIG), Chinese Academy of Sciences, as GSA: CRA001248, which is publicly accessible at <http://bigd.big.ac.cn/gsa>.

Authors’ contributions

XL and QS conceived and designed the project. JC, HS, XC, and Y-JZ performed aNSC culture, neurogenesis assay, m⁶A dot-blot, RT-PCR, and Western blot assays. JC, YZ, CH, and BS performed RNA-seq and MeRIP-seq data analysis. YY did RNA-seq and MeRIP-seq library construction. XL, JC, YZ, BS, YY, YGY, and QS analyzed the data. XL and YY wrote the manuscript with input from all other authors. All authors had read and approved the final manuscript.

Competing interests

The authors declared no competing financial interests.

Acknowledgments

XL was supported in part by the International Collaboration Program of the Ministry of Science and Technology of China (Grant No. YS2017YFGH001214), the National Natural Science Foundation of China (Grant Nos. 31771395 and 31571518), and the National Key R&D Program of China (Grant No. 2016YFC0900400). YY was supported by the National Natural Science Foundation of China (Grant No. 31770872), the Youth Innovation Promotion Association (Grant No. CAS2018133) and the National Key R&D Program of China, Stem Cell and Translational Research (Grant No. 2018YFA0109700). QS was supported in part by the National Key R&D Program of China (Grant No. 2017YFC1001703), the Key R&D Program of Zhejiang Province (Grant No. 2017C03009), and Zhejiang Provincial Program for the Cultivation of High-level Innovative Health Talents (2016-6), China.

Supplementary material

Supplementary data to this article can be found online at <https://doi.org/10.1016/j.gpb.2018.12.007>.

References

- [1] Christian KM, Song H, Ming GL. Functions and dysfunctions of adult hippocampal neurogenesis. *Annu Rev Neurosci* 2014;37:243–62.
- [2] Zhao C, Deng W, Gage FH. Mechanisms and functional implications of adult neurogenesis. *Cell* 2008;132:645–60.
- [3] Ming GL, Song H. Adult neurogenesis in the mammalian central nervous system. *Annu Rev Neurosci* 2005;28:223–50.
- [4] Goncalves JT, Schafer ST, Gage FH. Adult neurogenesis in the hippocampus: from stem cells to behavior. *Cell* 2016;167:897–914.
- [5] Li X, Jin P. Roles of small regulatory RNAs in determining neuronal identity. *Nat Rev Neurosci* 2010;11:329–38.
- [6] Yao B, Christian KM, He C, Jin P, Ming GL, Song H. Epigenetic mechanisms in neurogenesis. *Nat Rev Neurosci* 2016;17:537–49.
- [7] Ma DK, Marchetto MC, Guo JU, Ming GL, Gage FH, Song H. Epigenetic choreographers of neurogenesis in the adult mammalian brain. *Nat Neurosci* 2010;13:1338–44.
- [8] Sun W, Guan M, Li X. 5-hydroxymethylcytosine-mediated DNA demethylation in stem cells and development. *Stem Cells Dev* 2014;23:923–30.
- [9] Avgustinova A, Benitah SA. Epigenetic control of adult stem cell function. *Nat Rev Mol Cell Biol* 2016;17:643–58.
- [10] Atlasi Y, Stunnenberg HG. The interplay of epigenetic marks during stem cell differentiation and development. *Nat Rev Genet* 2017;18:643–58.
- [11] Hsieh J, Zhao X. Genetics and epigenetics in adult neurogenesis. *Cold Spring Harb Perspect Biol* 2016;8.
- [12] Li S, Mason CE. The pivotal regulatory landscape of RNA modifications. *Annu Rev Genomics Hum Genet* 2014;15:127–50.
- [13] Fu Y, Luo GZ, Chen K, Deng X, Yu M, Han D, et al. *N⁶*-methyldeoxyadenosine marks active transcription start sites in *Chlamydomonas*. *Cell* 2015;161:879–92.
- [14] Fustin JM, Doi M, Yamaguchi Y, Hida H, Nishimura S, Yoshida M, et al. RNA-methylation-dependent RNA processing controls the speed of the circadian clock. *Cell* 2013;155:793–806.
- [15] Meyer KD, Patil DP, Zhou J, Zinoviev A, Skabkin MA, Elemento O, et al. 5'UTR *m⁶A* promotes cap-independent translation. *Cell* 2015;163:999–1010.
- [16] Meyer KD, Saletore Y, Zumbo P, Elemento O, Mason CE, Jaffrey SR. Comprehensive analysis of mRNA methylation reveals enrichment in 3'UTRs and near stop codons. *Cell* 2012;149:1635–46.
- [17] Yoon KJ, Ringeling FR, Vissers C, Jacob F, Pokrass M, Jimenez-Cyrus D, et al. Temporal control of mammalian cortical neurogenesis by *m⁶A* methylation. *Cell* 2017;171:877–89.
- [18] Batista PJ, Molinie B, Wang J, Qu K, Zhang J, Li L, et al. *m⁶A* RNA modification controls cell fate transition in mammalian embryonic stem cells. *Cell Stem Cell* 2014;15:707–19.
- [19] Yue Y, Liu J, He C. RNA *N⁶*-methyladenosine methylation in post-transcriptional gene expression regulation. *Genes Dev* 2015;29:1343–55.
- [20] Lin S, Gregory RI. Methyltransferases modulate RNA stability in embryonic stem cells. *Nat Cell Biol* 2014;16:129–31.
- [21] Lence T, Akhtar J, Bayer M, Schmid K, Spindler L, Ho CH, et al. *m⁶A* modulates neuronal functions and sex determination in *Drosophila*. *Nature* 2016;540:242–7.
- [22] Zhao X, Yang Y, Sun BF, Shi Y, Yang X, Xiao W, et al. FTO-dependent demethylation of *N⁶*-methyladenosine regulates mRNA splicing and is required for adipogenesis. *Cell Res* 2014;24:1403–19.
- [23] Wang Y, Li Y, Toth JI, Petroski MD, Zhang Z, Zhao JC. *N⁶*-methyladenosine modification destabilizes developmental regulators in embryonic stem cells. *Nat Cell Biol* 2014;16:191–8.
- [24] Li HB, Tong J, Zhu S, Batista PJ, Duffy EE, Zhao J, et al. *m⁶A* mRNA methylation controls T cell homeostasis by targeting the *IL-7/STAT5/SOCS* pathways. *Nature* 2017;548:338–42.
- [25] Zhang C, Chen Y, Sun B, Wang L, Yang Y, Ma D, et al. *m⁶A* modulates haematopoietic stem and progenitor cell specification. *Nature* 2017;549:273–6.
- [26] Sevgi M, Rigoux L, Kuhn AB, Mauer J, Schilbach L, Hess ME, et al. An obesity-predisposing variant of the *FTO* gene regulates D2R-dependent reward learning. *J Neurosci* 2015;35:12584–92.
- [27] Hess ME, Hess S, Meyer KD, Verhagen LA, Koch L, Bronneke HS, et al. The fat mass and obesity associated gene (*Fto*) regulates activity of the dopaminergic midbrain circuitry. *Nat Neurosci* 2013;16:1042–8.
- [28] Nainar S, Marshall PR, Tyler CR, Spitale RC, Bredy TW. Evolving insights into RNA modifications and their functional diversity in the brain. *Nat Neurosci* 2016;19:1292–8.
- [29] Widagdo J, Zhao QY, Kempen MJ, Tan MC, Ratnu VS, Wei W, et al. Experience-dependent accumulation of *N⁶*-methyladenosine in the prefrontal cortex is associated with memory processes in mice. *J Neurosci* 2016;36:6771–7.
- [30] Li L, Zang L, Zhang F, Chen J, Shen H, Shu L, et al. Fat mass and obesity-associated (*FTO*) protein regulates adult neurogenesis. *Hum Mol Genet* 2017;26:2398–411.
- [31] Yu J, Chen M, Huang H, Zhu J, Song H, Zhu J, et al. Dynamic *m⁶A* modification regulates local translation of mRNA in axons. *Nucleic Acids Res* 2018;46:1412–23.
- [32] Merkurjev D, Hong WT, Iida K, Oomoto I, Goldie BJ, Yamaguti H, et al. Synaptic *N⁶*-methyladenosine (*m⁶A*) epitranscriptome reveals functional partitioning of localized transcripts. *Nat Neurosci* 2018;21:1004–14.
- [33] Li M, Zhao X, Wang W, Shi H, Pan Q, Lu Z, et al. Ythdf2-mediated *m⁶A* mRNA clearance modulates neural development in mice. *Genome Biol* 2018;19:69.
- [34] Ma C, Chang M, Lv H, Zhang ZW, Zhang W, He X, et al. RNA *m⁶A* methylation participates in regulation of postnatal development of the mouse cerebellum. *Genome Biol* 2018;19:68.

- [35] Engel M, Eggert C, Kaplick PM, Eder M, Roh S, Tietze L, et al. The role of m⁶A/m-RNA methylation in stress response regulation. *Neuron* 2018;99:389–403.e9.
- [36] Li X, Yao B, Chen L, Kang Y, Li Y, Cheng Y, et al. Ten-eleven translocation 2 interacts with forkhead box O3 and regulates adult neurogenesis. *Nat Commun* 2017;8:15903.
- [37] Szulwach KE, Li X, Smrt RD, Li Y, Luo Y, Lin L, et al. Cross talk between microRNA and epigenetic regulation in adult neurogenesis. *J Cell Biol* 2010;189:127–41.
- [38] Wang Y, Li Y, Yue M, Wang J, Kumar S, Wechsler-Reya RJ, et al. N⁶-methyladenosine RNA modification regulates embryonic neural stem cell self-renewal through histone modifications. *Nat Neurosci* 2018;21:195–206.
- [39] Zhang J, Ji F, Liu Y, Lei X, Li H, Ji G, et al. Ezh2 regulates adult hippocampal neurogenesis and memory. *J Neurosci* 2014;34:5184–99.
- [40] Pereira JD, Sansom SN, Smith J, Dobenecker MW, Tarakhovskiy A, Livesey FJ. Ezh2, the histone methyltransferase of PRC2, regulates the balance between self-renewal and differentiation in the cerebral cortex. *Proc Natl Acad Sci U S A* 2010;107:15957–62.
- [41] Cui Q, Shi H, Ye P, Li L, Qu Q, Sun G, et al. m⁶A RNA methylation regulates the self-renewal and tumorigenesis of glioblastoma stem cells. *Cell Rep* 2017;18:2622–34.
- [42] Geula S, Moshitch-Moshkovitz S, Dominissini D, Mansour AA, Kol N, Salmon-Divon M, et al. m⁶A mRNA methylation facilitates resolution of naive pluripotency toward differentiation. *Science* 2015;347:1002–6.
- [43] Satterlee JS, Basanta-Sanchez M, Blanco S, Li JB, Meyer K, Pollock J, et al. Novel RNA modifications in the nervous system: form and function. *J Neurosci* 2014;34:15170–7.
- [44] Meyer KD, Jaffrey SR. The dynamic epitranscriptome: N⁶-methyladenosine and gene expression control. *Nat Rev Mol Cell Biol* 2014;15:313–26.
- [45] Roignant JY, Soller M. m⁶A in mRNA: an ancient mechanism for fine-tuning gene expression. *Trends Genet* 2017;33:380–90.
- [46] Adhikari S, Xiao W, Zhao YL, Yang YG. m(6)A: signaling for mRNA splicing. *RNA Biol* 2016;13:756–9.
- [47] Koranda JL, Dore L, Shi H, Patel MJ, Vaasjo LO, Rao MN, et al. *Mettl14* is essential for epitranscriptomic regulation of striatal function and learning. *Neuron* 2018;99:283–92.e5.
- [48] Qiao H, Li Y, Feng C, Duo S, Ji F, Jiao J. *Nap1l1* controls embryonic neural progenitor cell proliferation and differentiation in the developing brain. *Cell Rep* 2018;22:2279–93.
- [49] Dominissini D, Moshitch-Moshkovitz S, Schwartz S, Salmon-Divon M, Ungar L, Osenberg S, et al. Topology of the human and mouse m⁶A RNA methylomes revealed by m⁶A-seq. *Nature* 2012;485:201–6.
- [50] Bolger AM, Lohse M, Usadel B. Trimmomatic: a flexible trimmer for Illumina sequence data. *Bioinformatics* 2014;30:2114–20.
- [51] Kim D, Perteza G, Trapnell C, Pimentel H, Kelley R, Salzberg SL. TopHat2: accurate alignment of transcriptomes in the presence of insertions, deletions and gene fusions. *Genome Biol* 2013;14:R36.
- [52] Zhang Y, Liu T, Meyer CA, Eeckhoutte J, Johnson DS, Bernstein BE, et al. Model-based analysis of ChIP-Seq (MACS). *Genome Biol* 2008;9:R137.
- [53] Quinlan AR, Hall IM. BEDTools: a flexible suite of utilities for comparing genomic features. *Bioinformatics* 2010;26:841–2.
- [54] Anders S, Pyl PT, Huber W. HTSeq—a Python framework to work with high-throughput sequencing data. *Bioinformatics* 2015;31:166–9.
- [55] Heinz S, Benner C, Spann N, Bertolino E, Lin YC, Laslo P, et al. Simple combinations of lineage-determining transcription factors prime cis-regulatory elements required for macrophage and B cell identities. *Mol Cell* 2010;38:576–89.
- [56] Wang L, Feng Z, Wang X, Wang X, Zhang X. DEGseq: an R package for identifying differentially expressed genes from RNA-seq data. *Bioinformatics* 2010;26:136–8.
- [57] Dennis Jr G, Sherman BT, Hosack DA, Yang J, Gao W, Lane HC, et al. DAVID: database for annotation, visualization, and integrated discovery. *Genome Biol* 2003;4:P3.
- [58] Shannon P, Markiel A, Ozier O, Baliga NS, Wang JT, Ramage D, et al. Cytoscape: a software environment for integrated models of biomolecular interaction networks. *Genome Res* 2003;13:2498–504.
- [59] Szklarczyk D, Morris JH, Cook H, Kuhn M, Wyder S, Simonovic M, et al. The STRING database in 2017: quality-controlled protein-protein association networks, made broadly accessible. *Nucleic Acids Res* 2017;45:D362–8.
- [60] Wang Y, Song F, Zhu J, Zhang S, Yang Y, Chen T, et al. GSA: genome sequence archive. *Genomics Proteomics Bioinformatics* 2017;15:14–8.
- [61] BIG Data Center Members. The BIG data center: from deposition to integration to translation. *Nucleic Acids Res* 2017;45:D18–24.